

Chebyshev HOPGD with Sparse Grid Sampling for Parameterized Linear Systems

SIOBHÁN CORRENTY*, MELINA A. FREITAG†, AND KIRK M. SOODHALTER‡

Abstract. We consider approximating solutions to parameterized linear systems of the form $A(\mu_1, \mu_2)x(\mu_1, \mu_2) = b$, where $(\mu_1, \mu_2) \in \mathbb{R}^2$. Here the matrix $A(\mu_1, \mu_2) \in \mathbb{R}^{n \times n}$ is nonsingular, large, and sparse and depends nonlinearly on the parameters μ_1 and μ_2 . Specifically, the system arises from a discretization of a partial differential equation and $x(\mu_1, \mu_2) \in \mathbb{R}^n$, $b \in \mathbb{R}^n$. This work combines companion linearization with the Krylov subspace method preconditioned bi-conjugate gradient (BiCG) and a decomposition of a tensor matrix of precomputed solutions, called snapshots. As a result, a reduced order model of $x(\mu_1, \mu_2)$ is constructed, and this model can be evaluated in a cheap way for many values of the parameters. Tensor decompositions performed on a set of snapshots can fail to reach a certain level of accuracy, and it is not known a priori if a decomposition will be successful. Moreover, the selection of snapshots can affect both the quality of the produced model and the computation time required for its construction. This new method offers a way to generate a new set of solutions on the same parameter space at little additional cost. An interpolation of the model is used to produce approximations on the entire parameter space, and this method can be used to solve a parameter estimation problem. Numerical examples of a parameterized Helmholtz equation show the competitiveness of our approach. The simulations are reproducible, and the software is available online.

Key words. Krylov methods, companion linearization, shifted linear systems, reduced order model, tensor decomposition, parameter estimation

AMS subject classifications. 65F10, 65N22, 65F55

1. Introduction. We are interested in approximating solutions to linear systems of the form

$$(1.1) \quad A(\mu_1, \mu_2)x(\mu_1, \mu_2) = b,$$

for many different values of the parameters μ_1, μ_2 . Here $A(\mu_1, \mu_2) \in \mathbb{R}^{n \times n}$ is a large and sparse nonsingular matrix with a nonlinear dependence on $\mu_1 \in [a_1, b_1] \subset \mathbb{R}$ and $\mu_2 \in [a_2, b_2] \subset \mathbb{R}$ and $x(\mu_1, \mu_2) \in \mathbb{R}^n$, $b \in \mathbb{R}^n$. Further, the system matrix arises from a discretization of a parameterized partial differential equation (PDE) and can be expressed as the sum of products of matrices and functions, i.e.,

$$(1.2) \quad A(\mu_1, \mu_2) = A_0 + A_1 f_1(\mu_1, \mu_2) + \dots + A_{n_f} f_{n_f}(\mu_1, \mu_2),$$

where $n_f \ll n$ and f_1, \dots, f_{n_f} are nonlinear scalar functions in the parameters μ_1 and μ_2 .

This work combines companion linearization, a technique from the study of nonlinear eigenvalue problems, with the Krylov subspace method bi-conjugate gradient (BiCG) [18, 23] and a tensor decomposition to construct a reduced order model. This smaller model can be evaluated inexpensively to approximate the solution to (1.1) for many values of the parameters. Additionally, the model can be used to solve a parameter estimation problem, i.e., to simultaneously estimate μ_1 and μ_2 for a given solution vector where these parameters are not known.

*Department of Mathematics, Royal Institute of Technology (KTH), SeRC Swedish e-Science Research Center, Lindstedtsvägen 25, Stockholm, Sweden correnty@kth.se

†Institute of Mathematics, University of Potsdam, Karl-Liebknecht-Str. 24-25, 14476 Potsdam, Germany melina.freitag@uni-potsdam.de

‡School of Mathematics, Trinity College Dublin, The University of Dublin, College Green, Dublin 2, Ireland ksoodha@maths.tcd.ie

More specifically, our proposed method is based on a decomposition of a tensor matrix of precomputed solutions to (1.1), called snapshots. In this way, building the reduced order model can be divided into two main parts:

1. Generate the snapshots for many pairs (μ_1, μ_2) .
2. Perform the tensor decomposition.

There have been many prior works which rely on *sampling*; see, e.g., [7, 8, 25, 26, 27, 28]. In particular, solutions corresponding to each (μ_1, μ_2) in the tensor matrix are obtained by solving the linear systems individually. Here, we instead obtain the snapshots with the method proposed in [14], Preconditioned Chebyshev BiCG for parameterized linear systems. This choice allows for great flexibility in the selection of the set of snapshots included in the tensor, as the approximations are generated as one variable *functions* of μ_1 or of μ_2 , i.e., with one parameter fixed. These functions are cheap to evaluate for different values of the parameter, and this method is described in Section 2.

The tensor matrix of precomputed snapshots has a particular structure, as we consider sampling on a structured, sparse grid in the parameter space. This is a way to overcome the so-called *curse of dimensionality*, since the number of snapshots to generate and store grows exponentially with the dimension when the sampling is performed on a conventional full grid. The decomposition is performed with a variant of the higher-order proper generalized decomposition (HOPGD), as proposed in [25].¹ The approach here has been adapted for this particular setting with fewer snapshots and, as in the standard implementation, results in a separated expression in μ_1 and μ_2 . Once constructed, the decomposition is interpolated to approximate solutions to (1.1) corresponding to all parameters $(\mu_1, \mu_2) \in [a_1, b_1] \times [a_2, b_2]$.

In general, we cannot guarantee that the error in a tensor decomposition for a certain set of snapshots will reach a specified accuracy level. Further, it is not known a priori which sets of snapshots will lead to a successful decomposition, even with modest standards for the convergence [21]. Different selections of snapshots can lead to models which are more efficient to compute and more robust overall, but the optimal set is not known beforehand. Moreover, generating the snapshots is the *dominating cost* of building the reduced order model. In instances where the decomposition process fails to converge or yields an inadequate model, our proposed method provides an effective remedy. It facilitates the generation of a new set of snapshots within the same parameter space $[a_1, b_1] \times [a_2, b_2]$ with *little extra computation*. These snapshots can be used to construct a new reduced order model for the same parameter space in an identical way. This is the main contribution developed in this work; we refer to Section 4 for additional elaboration.

More precisely, an alternating directions, greedy algorithm is used to perform the decomposition, where the cost of each step of the method grows linearly with the number of unknowns n . The basis vectors for the decomposition are not known beforehand, similar to the established proper generalized decomposition (PGD), often used to create reduced order models of PDEs which are separated in the time and space variables. The method PGD has been used widely in the study of highly nonlinear PDEs [11, 12, 13] and has been generalized to solve multiparametric problems; see, for instance, [5, 6].

Evaluating the resulting reduced order model is in general much more efficient than solving the systems individually for each choice of the parameters [25]. Reliable and accurate approximations are available for a variety of parameter choices,

¹The method HOPGD [28] decomposes a tensor of snapshots sampled on a full grid.

and parameter estimation can be performed in a similarly competitive way. Details regarding the construction of the reduced order model are found in Section 3, and numerical simulations of a parameterized Helmholtz equation and a parameterized advection-diffusion equation are presented in Sections 5 and 6, respectively. All experiments were carried out on a 2.3 GHz Dual-Core Intel Core i5 processor with 16 GB RAM, and the corresponding software can be found online.²

2. Generating snapshots with Preconditioned Chebyshev BiCG. Reduced order models based on sampling of snapshot solutions are typically constructed generating many finite element approximations individually in an offline stage. We base our approach to obtain the snapshot solutions $x(\mu_1, \mu_2)$ to (1.1) on an adapted version of the Preconditioned Chebyshev BiCG method for parameterized linear systems, originally proposed in [14]. Here, the unique solution to a companion linearization, formed from a Chebyshev approximation using `Chebfun` [15], is generated in a preconditioned BiCG [18, 23] setting. Two executions of this method generate all finite element solutions corresponding to the values of the parameters shown in Figure 3.2. Specifically, one execution for *all solutions* on the line $\mu_1 = \mu_1^*$ and one execution for *all solutions* on the line $\mu_2 = \mu_2^*$ in the plane $[a_1 \times b_1] \times [a_2 \times b_2]$. In this way, we generate solutions fixed in one parameter. Moreover, the sampling represented here is sufficient to build a reliable reduced order model with the strategy presented in [25]. We briefly summarize this method as follows.

A Chebyshev approximation of $A(\mu_1, \mu_2)$ for a fixed $\mu_2^* \in \mathbb{R}$ is given by $P(\mu_1)$, where

$$(2.1) \quad A(\mu_1, \mu_2^*) \approx P(\mu_1) := P_0\tau_0(\mu_1) + \dots + P_d\tau_d(\mu_1).$$

Here τ_ℓ is the degree ℓ Chebyshev polynomial on $[-c_1, c_1]$ and $P_\ell \in \mathbb{R}^{n \times n}$ are the corresponding interpolation coefficients. Note, $c_l \in \mathbb{R}$ is chosen such that $[a_l, b_l] \subseteq [-c_l, c_l]$, for $l = 1, 2$. A companion linearization based on the linear system

$$(2.2) \quad P(\mu_1)\hat{x}(\mu_1) = b$$

with $\hat{x}(\mu_1) = \hat{x}(\mu_1, \mu_2^*) \approx x(\mu_1, \mu_2^*)$, where $x(\mu_1, \mu_2^*)$ is as in (1.1), and a fixed μ_2^* has the form

$$(2.3) \quad (K - \mu_1 M)u(\mu_1) = c,$$

where $K, M \in \mathbb{R}^{dn \times dn}$ are coefficient matrices, independent of the parameter μ_1 , $c \in \mathbb{R}^{dn}$ is a constant vector, and the solution $u(\mu_1)$ is unique. This linearization, inspired by the work [16] and studied fully in [14], relies on the well-known three-term recurrence of the Chebyshev polynomials.

Solutions to the systems in (2.3) are approximated with the Krylov subspace method bi-conjugate gradient for shifted systems [2, 19]. Specifically, we approximate an equivalent shifted system, preconditioned with $(K - \sigma M)^{-1}$, given by

$$(2.4a) \quad (K - \mu_1 M)(K - \sigma M)^{-1}\hat{u}(\mu_1) = c$$

$$(2.4b) \quad \iff (I + (-\mu_1 + \sigma)M(K - \sigma M)^{-1})\hat{u}(\mu_1) = c,$$

where $\hat{u}(\mu_1) = (K - \sigma M)u(\mu_1)$. The k th approximation comes from the Krylov subspace generated from the matrix $M(K - \sigma M)^{-1}$ and the vector c , defined by

$$(2.5) \quad \mathcal{K}_k := \text{span}\{c, M(K - \sigma M)^{-1}c, \dots, (M(K - \sigma M)^{-1})^{k-1}c\},$$

²<https://github.com/siobhanie/ChebyshevHOPGD>

where $\mathcal{K}_k = \mathcal{K}_k(M(K - \sigma M)^{-1}, c)$. In particular, the method exploits the shift- and scaling- invariance properties of Krylov subspaces, and the preconditioner is applied efficiently based on the prior works [4, 22].

A Lanczos biorthogonalization process generates a basis matrix $V_k \in \mathbb{R}^{dn \times k}$ for (2.5) and a tridiagonal matrix $T_k \in \mathbb{R}^{k \times k}$ such that

$$M(K - \sigma M)^{-1}V_k = V_k T_k + \beta_k v_{k+1} e_k^T$$

holds, where $\beta_k \in \mathbb{R}$, I_k is the identity matrix of dimension k , and e_k is the k th column of I_k . Further, v_{k+1} is the $(k+1)$ th column in the basis matrix for \mathcal{K}_{k+1} .

Approximations to (2.3) and, equivalently, approximations to (1.1), can be computed efficiently for μ_1^i , $i = 1, \dots, n_1$, as follows:

$$(2.6a) \quad y_k(\mu_1^i) = (I_k + (-\mu_1^i + \sigma T_k))^{-1} (\beta e_1),$$

$$(2.6b) \quad z_k(\mu_1^i) = V_k y_k(\mu_1^i),$$

$$(2.6c) \quad x_k(\mu_1^i, \mu_2^*) = ((K - \sigma M)^{-1} z_k(\mu_1^i))_{1:n}.$$

Here, $\beta := \|b\|$, where b is as in (1.1), and $x_k(\mu_1, \mu_2^*)$ denotes the approximation to (1.1) from the Krylov subspace (2.5) of dimension k corresponding to (μ_1, μ_2^*) . Equivalently, $x_k(\mu_1, \mu_2^*) \approx \hat{x}(\mu_1, \mu_2^*)$, where $\hat{x}(\mu_1, \mu_2^*)$ is the solution to the system (2.2). Note, the subscript on the right-hand side of (2.6c) denotes the first n elements in the vector.

Since $k \ll n$, solving the tridiagonal system in (2.6a) is not computationally demanding. As a result, once we build a sufficiently large Krylov subspace via one execution of the main algorithm, we have access to approximations $x_k(\mu_1^i, \mu_2^*)$ for all μ_1^i in the interval $[a_1, b_1]$. The process of approximating (1.1) for a fixed μ_1^i and μ_2^j , for $j = 1, \dots, n_2$, is completely analogous to the above procedure and, thus, we have access to approximations $x_k(\mu_1^i, \mu_2^j)$ for all μ_2^j on the interval $[a_2, b_2]$, obtained in a similarly efficient way.

REMARK 2.1 (Choice of target parameter). *The use of shift-and-invert preconditioners with well-chosen σ generally result in fast convergence, i.e., a few iterations of the shifted BiCG algorithm. This is because $(K - \mu_1 M)(K - \sigma M)^{-1} \approx I$, for $\mu_1 \approx \sigma$.*

3. Sparse grid based HOPGD. Let $X(\mu_1, \mu_2) \in \mathbb{R}^{n \times n_1 \times n_2}$ be a sparse, three-dimensional tensor of approximations to (1.1). These precomputed snapshots, generated by two executions of the preconditioned Krylov subspace method described in Section 2, correspond to the pairs of parameters (μ_1^i, μ_2^*) , $i = 1, \dots, n_1$, and (μ_1^*, μ_2^j) , $j = 1, \dots, n_2$. Here, μ_1^i are in the interval $[a_1, b_1]$, μ_2^j are in the interval $[a_2, b_2]$, and $\mu_1^* \in [a_1, b_1]$, $\mu_2^* \in [a_2, b_2]$ are fixed values. More precisely,

$$(3.1a) \quad X(\mu_1^i, \mu_2^*) = \hat{x}(\mu_1^i, \mu_2^*) \in \mathbb{R}^n, \quad i = 1, \dots, n_1,$$

$$(3.1b) \quad X(\mu_1^*, \mu_2^j) = \tilde{x}(\mu_1^*, \mu_2^j) \in \mathbb{R}^n, \quad j = 1, \dots, n_2,$$

and the remaining entries of $X(\mu_1, \mu_2)$ are zeros; see Figure 3.1 for a visualization of a tensor of this form. Note, $\hat{x}(\mu_1^i, \mu_2^*) = \hat{x}(\mu_1^i)$ are approximations to the linear systems $A(\mu_1^i, \mu_2^*)x(\mu_1^i, \mu_2^*) = b$ and $\tilde{x}(\mu_1^*, \mu_2^j) = \tilde{x}(\mu_2^j)$ approximate solutions to $A(\mu_1^*, \mu_2^j)x(\mu_1^*, \mu_2^j) = b$. We refer to the set

$$(3.2) \quad \mu := \{(\mu_1^i, \mu_2^*) : i = 1, \dots, n_1\} \cup \{(\mu_1^*, \mu_2^j) : j = 1, \dots, n_2\}$$

as the *nodes* and $\boldsymbol{\mu} \subset [a_1, b_1] \times [a_2, b_2]$. The set of nodes corresponding to the tensor matrix $X(\mu_1, \mu_2)$ in Figure 3.1 are visualized in Figure 3.2. This way of sampling in the parameter space is a way to mitigate the so-called *curse of dimensionality* in terms of the number of snapshots to generate and store.

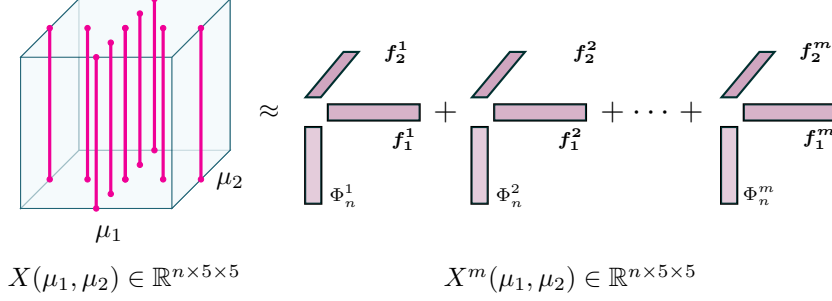


FIG. 3.1. Example of tensor matrix $X(\mu_1, \mu_2)$ consisting of 9 snapshot solutions (dots connected by vertical lines) and reduced order model $X^m(\mu_1, \mu_2)$ of rank m as in (3.3), where $\Phi_n^k \in \mathbb{R}^n$, $\mathbf{f}_1^k := [F_1^k(\mu_1^1), \dots, F_1^k(\mu_1^5)] \in \mathbb{R}^5$, $\mathbf{f}_2^k := [F_2^k(\mu_2^1), \dots, F_2^k(\mu_2^5)] \in \mathbb{R}^5$. Approximation is sum of rank-one tensors.

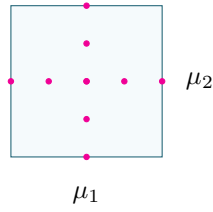


FIG. 3.2. Sampling on a sparse grid in the parameter space. Nodes (3.2) correspond to the 9 snapshot solutions in Figure 3.1 with $\mu_1 \in [a_1, b_1]$, $\mu_2 \in [a_2, b_2]$, $\mu_1^* = (a_1 + b_1)/2$, $\mu_2^* = (a_2 + b_2)/2$. All snapshots generated via two executions of Preconditioned Chebyshev BiCG.

Sparse grid based higher order proper generalized decomposition (HOPGD) [25] is a method which generates a tensor $X^m(\mu_1, \mu_2) \in \mathbb{R}^{n \times n_1 \times n_2}$ to approximate $X(\mu_1, \mu_2)$. Specifically, the approximations are separated in the parameters μ_1 and μ_2 and, at each pair of parameters in (3.2), are of the form

$$(3.3a) \quad X(\mu_1^i, \mu_2^*) \approx X^m(\mu_1^i, \mu_2^*) = \sum_{k=1}^m \Phi_n^k F_1^k(\mu_1^i) F_2^k(\mu_2^*) \in \mathbb{R}^n, \quad i = 1, \dots, n_1,$$

$$(3.3b) \quad X(\mu_1^*, \mu_2^j) \approx X^m(\mu_1^*, \mu_2^j) = \sum_{k=1}^m \Phi_n^k F_1^k(\mu_1^*) F_2^k(\mu_2^j) \in \mathbb{R}^n, \quad j = 1, \dots, n_2,$$

where $\Phi_n^k \in \mathbb{R}^n$ and

$$(3.4) \quad F_1^k : \mathbb{R} \rightarrow \mathbb{R}, \quad F_2^k : \mathbb{R} \rightarrow \mathbb{R}$$

are one variable scalar functions of the parameters μ_1 and μ_2 , respectively. Here m is the rank of the approximation and F_l^k , $l = 1, 2$, are the unknown functions of the k th mode. In this way, the nonzero entries of the tensor $X(\mu_1, \mu_2)$ are estimated by a linear combination involving products of lower-dimensional functions.

The decomposition in (3.3) generates only the evaluations of F_l^k , and the reduced basis vectors for the approximation are not known a priori. Instead, these vectors are determined on-the-fly, in contrast to other methods based on the similar proper orthogonal decomposition [7, 12]. A visualization of this decomposition on a sparse tensor of snapshots appears in Figure 3.1. The spacing of the nodes is equidistant in both the μ_1 and μ_2 directions, conventional for methods of this type.

We note the similarity between this method and the well-known higher-order singular value decomposition (HOSVD) [24]. Additionally, the reduced order model generated via the method sparse grid based HOPGD and visualized in Figure 3.1 is of the same form as the established CANDECOMP/PARAFAC (CP) decomposition, i.e., the approximations consists of a sum of rank-one tensors [21].

The model as expressed in (3.3) can only be evaluated on the set of nodes (3.2) corresponding to the snapshots included in the tensor matrix (3.1). To access other approximations, interpolations of F_l^k will be required; see Section 3.2. The particular structure of the sampling incorporated here is very similar to that which is used in traditional sparse grid methods for PDEs [10]. Our approach *differs fundamentally* from these methods, which are based on an interpolation of high dimensional functions using a hierarchical basis. See [9] for a method in this style, where a reduced order model was constructed using hierarchical collocation to solve parameteric problems.

REMARK 3.1 (Evaluation of the model at a point in space). *The approximation in (3.3) is expressed using vectors of length n as the examples which follow in Sections 5 concern a parameterized PDE discretized on a spatial domain denoted by Ω . In particular, we are interested in the solutions to these PDEs for many values of the parameters μ_1 and μ_2 . The approximation (3.3), expressed at a point in space, is denoted by*

$$(3.5) \quad X(x_0, \mu_1, \mu_2) \approx X^m(x_0, \mu_1, \mu_2) = \sum_{k=1}^m \Phi^k(x_0) F_1^k(\mu_1) F_2^k(\mu_2) \in \mathbb{R},$$

for a particular $(\mu_1, \mu_2) \in \boldsymbol{\mu}$ (3.2), where $x_0 \in \Omega \subset \mathbb{R}^d$ is a spatial parameter, d is the dimension of the spatial domain, and $\Phi^k(x_0) \in \mathbb{R}$ is an entry of the vector $\Phi_n^k \in \mathbb{R}^n$ in (3.3). Specifically, Φ_n^k denotes Φ^k evaluated on a set of n spatial discretization points Ω_{dp} , where $\Omega_{dp} \subset \Omega$. As in (3.3), to evaluate the model in (3.5) for values of μ_1 and μ_2 outside of the set of nodes, interpolations must be performed.

3.1. Computation of the separated expression. Traditionally, tensor decomposition methods require sampling performed on full grids in the parameter space, requiring the computation and storage of many snapshot solutions. See [8, 26, 28] for HOPGD performed in this setting, as well as an example in Section 5.2. The tensor decomposition proposed in [25] is specifically designed for sparse tensors. In particular, the sampling is of the same form considered in Section 2 and shown in Figures 3.1 and 3.2. This approach is more efficient, as it requires fewer snapshots and, as a result, the decomposition is performed in fewer computations. The method in [25], adapted to our particular setting, is briefly summarized here.

We seek an approximation to the nonzero vertical columns of $X(\mu_1, \mu_2)$ described in (3.1), separated in the parameters $\mu_1 \in [a_1, b_1]$ and $\mu_2 \in [a_2, b_2]$. The full parameter domain is defined by $\mathcal{D} := \Omega \times [a_1, b_1] \times [a_2, b_2]$, where $\Omega \subset \mathbb{R}^d$. We express solutions

as vectors of length n , i.e., as approximations to (1.1) evaluated at a particular node (μ_1, μ_2) ; cf. (3.5), where solutions are expressed at a single point in the spatial domain. The approximations satisfy

$$\begin{aligned}
(3.6a) \quad X(\mu_1, \mu_2) &\approx X^m(\mu_1, \mu_2) \\
(3.6b) \quad &= \sum_{k=1}^m \Phi_n^k F_1^k(\mu_1) F_2^k(\mu_2) \\
(3.6c) \quad &= X^{m-1}(\mu_1, \mu_2) + \Phi_n^m F_1^m(\mu_1) F_2^m(\mu_2),
\end{aligned}$$

for $(\mu_1, \mu_2) \in \boldsymbol{\mu}$, where $\boldsymbol{\mu}$ is the set of nodes defined in (3.2), and are generated via an alternating directions strategy. Specifically, at each enrichment step m , all components $\Phi_n^m \in \mathbb{R}^n$, $F_1^m(\mu_1) \in \mathbb{R}$, $F_2^m(\mu_2) \in \mathbb{R}$ in (3.6c) are initialized then updated sequentially to construct an L^2 projection of $X(\mu_1, \mu_2)$. This is done via a greedy algorithm, where all components are assumed fixed, except the one we seek to compute. The process is equivalent to the minimization problem described as follows. At step m , find $X^m(\mu_1, \mu_2) \in V_m \subset L^2(\mathcal{D})$ as in (3.6) such that

$$(3.7) \quad \min_{X^m(\mu_1, \mu_2)} \left(\frac{1}{2} \|wX(\mu_1, \mu_2) - wX^m(\mu_1, \mu_2)\|_{L^2(\mathcal{D})}^2 \right),$$

where w is the sampling index, i.e.,

$$\begin{cases} w = 1, & (\mu_1, \mu_2) \in \boldsymbol{\mu}, \\ w = 0, & \text{otherwise,} \end{cases}$$

\mathcal{D} is the full parameter domain, and V_m represents a set of test functions. Equivalently, using the weak formulation, we seek the solution $X^m(\mu_1, \mu_2)$ to

$$(3.8) \quad (wX^m(\mu_1, \mu_2), \delta X)_{\mathcal{D}} = (wX(\mu_1, \mu_2), \delta X)_{\mathcal{D}}, \quad \forall \delta X \in V_m.$$

Here $(\cdot, \cdot)_{\mathcal{D}}$ denotes the integral of the scalar product over the domain \mathcal{D} , and (3.8) can be written as

$$(3.9) \quad (w\Phi_n^m F_1^m F_2^m, \delta X)_{\mathcal{D}} = (wX(\mu_1, \mu_2) - wX^{m-1}(\mu_1, \mu_2), \delta X)_{\mathcal{D}}, \quad \forall \delta X \in V_m.$$

We have simplified the notation in (3.9) with $F_1^m := F_1^m(\mu_1)$ and $F_2^m := F_2^m(\mu_2)$ for readability. In practice, approximations to (3.9) are computed successively via a least squares procedure until a fixed point is detected. The m th test function is given by $\delta X := \delta\Phi_n^m F_1^m F_2^m + \Phi_n^m \delta F_1^m F_2^m + \Phi_n^m F_1^m \delta F_2^m$, and the approximation (3.6c) is updated with the resulting components.

More concretely, let the initializations Φ_n^m , $\mathbf{f}_1^m := [F_1^m(\mu_1^1), \dots, F_1^m(\mu_1^{n_1})] \in \mathbb{R}^{n_1}$, $\mathbf{f}_2^m := [F_2^m(\mu_2^1), \dots, F_2^m(\mu_2^{n_2})] \in \mathbb{R}^{n_2}$ be given. We seek first an update of $\Phi_n^{m_{\text{old}}} := \Phi_n^m$, assuming $F_1^{m_{\text{old}}} := F_1^m$, $F_2^{m_{\text{old}}} := F_2^m$ are known function evaluations for all $(\mu_1, \mu_2) \in \boldsymbol{\mu}$. We update Φ_n^m as

$$(3.10) \quad \Phi_n^m = \frac{\sum_{\boldsymbol{\mu}} r_{m-1}(\mu_1, \mu_2)}{\sum_{\boldsymbol{\mu}} F_1^m(\mu_1) F_2^m(\mu_2)},$$

where the $(m-1)$ th residual vector is given by

$$(3.11) \quad r_{m-1}(\mu_1, \mu_2) := X(\mu_1, \mu_2) - X^{m-1}(\mu_1, \mu_2) \in \mathbb{R}^n.$$

Denote the vector obtained in (3.10) by $\Phi_n^{m_{\text{new}}}$ and seek an update of $F_1^{m_{\text{old}}}(\mu_1^i)$, assuming $\Phi_n^m, F_2^m(\mu_2^j)$ known, using

$$(3.12) \quad F_1^m(\mu_1^i) = \frac{(\Phi_n^m)^T r_{m-1}(\mu_1^i, \mu_2^*)}{(\Phi_n^m)^T \Phi_n^m F_2^m(\mu_2^*)},$$

for $i = 1, \dots, n_1$. We denote the solutions found in (3.12) by $F_1^{m_{\text{new}}}(\mu_1^i)$. Note, $\Phi_n^{m_{\text{new}}}$ and $F_2^{m_{\text{old}}}(\mu_2^j)$ are used in the computations in (3.12). The updates $F_2^m(\mu_2^j)$ are computed as

$$(3.13) \quad F_2^m(\mu_2^j) = \frac{(\Phi_n^m)^T r_{m-1}(\mu_1^*, \mu_2^j)}{(\Phi_n^m)^T \Phi_n^m F_1^m(\mu_1^*)},$$

for $j = 1, \dots, n_2$, which we denote by $F_2^{m_{\text{new}}}(\mu_2^j)$, where $\Phi_n^{m_{\text{new}}}$ and $F_1^{m_{\text{new}}}(\mu_1^i)$ were used in the computations in (3.13). For a certain tolerance level ε_1 , if the relation

$$(3.14) \quad \|\delta(\mu_1, \mu_2)\| < \varepsilon_1$$

holds for all $(\mu_1, \mu_2) \in \boldsymbol{\mu}$, where

$$(3.15) \quad \delta(\mu_1, \mu_2) := \Phi_n^{m_{\text{old}}} F_1^{m_{\text{old}}}(\mu_1) F_2^{m_{\text{old}}}(\mu_2) - \Phi_n^{m_{\text{new}}} F_1^{m_{\text{new}}}(\mu_1) F_2^{m_{\text{new}}}(\mu_2),$$

we have approached a fixed point. In this case, the approximation in (3.6c) is updated with the components $\Phi_n^m, F_1^m(\mu_1^i)$, and $F_2^m(\mu_2^j)$. If the condition (3.14) is not met, we set $\Phi_n^{m_{\text{old}}} := \Phi_n^{m_{\text{new}}}$, $F_1^{m_{\text{old}}}(\mu_1^i) := F_1^{m_{\text{new}}}(\mu_1^i)$, $F_2^{m_{\text{old}}}(\mu_2^j) := F_2^{m_{\text{new}}}(\mu_2^j)$ and repeat the process described above. If

$$\frac{\|X(\mu_1, \mu_2) - X^m(\mu_1, \mu_2)\|}{\|X(\mu_1, \mu_2)\|} < \varepsilon_2$$

is met for a specified ε_2 and all $(\mu_1, \mu_2) \in \boldsymbol{\mu}$, the algorithm terminates. Otherwise, we seek $\Phi_n^{m+1}, F_1^{m+1}(\mu_1^i), F_2^{m+1}(\mu_2^j)$ using the same procedure, initialized with the most recent updates. This process is summarized in Algorithm 1.

In general, decompositions of many sets of snapshots can be performed to an acceptable accuracy level with $m \ll n$, where the parameter m depends on the regularity of the exact solution [12]. Efficiency and robustness have been shown for the standard PGD method generated with a greedy algorithm like the one described here [13, 26, 31]. Note, the accuracy of the approximations here depends strongly on the quality of the separated functions in the model [25]. Additionally, the decomposition produced by the standard HOPGD method is optimal when the separation involves two parameters [28].

The reduced order model described here can be used to approximate solutions to (1.1) for many (μ_1, μ_2) outside of the set of nodes. This is achieved through interpolating the one variable functions in (3.4). Consider also a solution vector $x(\mu_1, \mu_2) \in \mathbb{R}^n$ to (1.1), where (μ_1, μ_2) are unknown. The interpolation of $X^m(\mu_1, \mu_2)$ can be used to estimate the parameters μ_1, μ_2 which produce this particular solution.

REMARK 3.2 (Separated expression in more than two parameters). *The reduced order model (3.3) is separated in the two parameters μ_1 and μ_2 . In [25], models separated in as many as six parameters were constructed, where the sampling was performed on a sparse grid in the parameter space. The authors note this particular approach for the decomposition may not be optimal in the sense of finding the best*

approximation, though it is possible. Our proposed way of computing the snapshots could be generalized to a setting separated in s parameters. In this way, the procedure would fix $(s-1)$ parameters at a time and execute Chebyshev BiCG a total of s times.

REMARK 3.3 (Comparison of HOPGD to similar methods). In [28], HOPGD was studied alongside the similar HOSVD method. The decompositions were separated in as many as six parameters, and the sampling was performed on a full grid in the parameter space. In general, HOPGD produced separable representations with fewer terms compared with HOSVD. In this way, the model constructed by HOPGD can be evaluated in a more efficient manner. Furthermore, the method HOPGD does not require the number of terms in the separated solution to be set a priori, as in a CP decomposition.

Algorithm 1: Chebyshev HOPGD with sparse grid sampling for parameterized linear systems

Input: Set of nodes $\boldsymbol{\mu}$ as in (3.2), tensor matrix of precomputed snapshots $X(\mu_1, \mu_2)$ as in (3.3), tolerances $\varepsilon_1, \varepsilon_2 > 0$
Output: Function $\mathbf{X}^m(\mu_1, \mu_2) : [a_1, b_1] \times [a_2, b_2] \rightarrow \mathbb{R}^n$, approx to (1.1)
Initialize: $\Phi_n^1 \in \mathbb{R}^n$, $F_1^1(\mu_1^i) \in \mathbb{R}$, $F_2^1(\mu_2^j) \in \mathbb{R}$, $i = 1, \dots, n_1$, $j = 1, \dots, n_2$

- 1 $m = 1$
- 2 Set $X^0(\mu_1^i, \mu_2^j) := 0$, $X^m(\mu_1^i, \mu_2^j) := \Phi_n^m F_1^m(\mu_1^i) F_2^m(\mu_2^j)$
- 3 **while** $\|X(\mu_1, \mu_2) - X^m(\mu_1, \mu_2)\| / \|X(\mu_1, \mu_2)\| > \varepsilon_2$, for any $(\mu_1, \mu_2) \in \boldsymbol{\mu}$ **do**
- 4 Set $\Phi_n^{m_{\text{old}}} := \Phi_n^m$, $F_1^{m_{\text{old}}}(\mu_1^i) := F_1^m(\mu_1^i)$, $F_2^{m_{\text{old}}}(\mu_2^j) := F_2^m(\mu_2^j)$
- 5 Compute Φ_n^m with (3.10)
- 6 Set $\Phi_n^{m_{\text{new}}} := \Phi_n^m$
- 7 Compute $F_1^m(\mu_1^i)$ with (3.12)
- 8 Set $F_1^{m_{\text{new}}}(\mu_1^i) := F_1^m(\mu_1^i)$
- 9 Compute $F_2^m(\mu_2^j)$ with (3.13)
- 10 Set $F_2^{m_{\text{new}}}(\mu_2^j) := F_2^m(\mu_2^j)$
- 11 Compute $\delta(\mu_1^i, \mu_2^j)$ using (3.15)
- 12 **if** $\delta(\mu_1, \mu_2) < \varepsilon_1$, for all $(\mu_1, \mu_2) \in \boldsymbol{\mu}$ **do**
- 13 Update $X^m(\mu_1, \mu_2)$ as in (3.6c)
- 14 Set $m := m + 1$
- 15 Set $\Phi_n^m := \Phi_n^{m-1}$, $F_1^m(\mu_1^i) := F_1^{m-1}(\mu_1^i)$, $F_2^m(\mu_2^j) := F_2^{m-1}(\mu_2^j)$
- 16 **end**
- 17 **end**
- 18 **return** Compute interpolation $\mathbf{X}^m(\mu_1, \mu_2)$ as in (3.16)

3.2. Interpolated model. The tensor representation in (3.3) consists, in part, of one-dimensional functions F_1^k and F_2^k , for $k = 1, \dots, m$. Note, we have only evaluations of these functions at μ_1^i , $i = 1, \dots, n_1$ and μ_2^j , $j = 1, \dots, n_2$, respectively, and no information about these functions outside of these points. In this way, we cannot approximate the solution to (1.1) for all $(\mu_1, \mu_2) \in [a_1, b_1] \times [a_2, b_2]$ using (3.3) as written.

We can use the evaluations $F_1^k(\mu_1^i)$ and $F_2^k(\mu_2^j)$ in (3.3) to compute an interpolation of these one-dimensional functions in a cheap way. In practice, any interpolation is possible and varying the type of interpolation does not contribute significantly to the overall error in the approximation. Thus, we make the following interpolation of

the representation in (3.3):

$$(3.16) \quad \mathbf{X}^m(\mu_1, \mu_2) = \sum_{k=1}^m \Phi_n^k \mathbf{F}_1^k(\mu_1) \mathbf{F}_2^k(\mu_2) \in \mathbb{R}^n,$$

where $\mathbf{F}_1^k, \mathbf{F}_2^k$ are spline interpolations of F_1^k, F_2^k (3.4), respectively, and $\mathbf{X}^m(\mu_1, \mu_2) : [a_1, b_1] \times [a_2, b_2] \rightarrow \mathbb{R}^n$. The interpolation in (3.16) can be evaluated to approximate (1.1) for other $(\mu_1, \mu_2) \in [a_1, b_1] \times [a_2, b_2]$ in a cheap way. This approximation to $x(\mu_1, \mu_2)$ is denoted as

$$(3.17) \quad x^m(\mu_1, \mu_2) \in \mathbb{R}^n,$$

and we compute the corresponding relative error as follows:

$$\frac{\|x^m(\mu_1, \mu_2) - x(\mu_1, \mu_2)\|_2}{\|x(\mu_1, \mu_2)\|_2}.$$

Note, simply interpolating several snapshots to estimate solutions to (1.1) for all (μ_1, μ_2) in the parameter space is not a suitable approach, as the solutions tend to be extremely sensitive to the parameters [28].

To solve the parameter estimation problem for a given solution $x(\mu_1, \mu_2) \in \mathbb{R}^n$ which depends on unknown parameters (μ_1, μ_2) , we use the MATLAB routine `fmincon`. This routine uses the sequential quadratic programming algorithm [30] to find the pair of values (μ_1, μ_2) in the parameter domain that minimizes the quantity

$$(3.18) \quad \|x(\mu_1, \mu_2) - x^m(\mu_1, \mu_2)\|_2.$$

Simulations from a parameterized Helmholtz equation and a parameterized advection-diffusion equation appear in Sections 5 and 6, respectively. In these experiments, an interpolation of a reduced order model is constructed to approximate the solutions to the parameterized PDEs.

REMARK 3.4 (Offline and online stages). *In practice, the fixed point method in Algorithm 1 can require many iterations until convergence, though the cost of each step scales linearly with the number of unknowns. Residual-based accelerators have been studied to reduce the number of these iterations [25]. This strategy, though outside the scope of this work, has shown to be beneficial in situations where the snapshots depended strongly on the parameters. Only one successful decomposition is required to construct (3.16). Thus, the offline stage of the method consists of generating the snapshots with Chebyshev BiCG and executing Algorithm 1.*

Evaluating the reduced order model (3.16) requires only scalar and vector operations and, therefore, a variety of approximations to (1.1) can be obtained very quickly, even when the number of unknowns is large. We consider this part of the proposed method the online stage. In the experiment corresponding to Figure 5.5, evaluating the reduced order model had simulation time 0.010601 CPU seconds. Generating the corresponding finite element solution with backslash in MATLAB had simulation time 1.197930 CPU seconds.

REMARK 3.5 (Sources of error). *The approximations generated by Algorithm 1 contain error from the Chebyshev approximation, the iterative method Preconditioned Chebyshev BiCG, the low-rank approximation, as well as the interpolations in (3.16). The Chebyshev approximation has a very small impact on the overall error, and Figure 5.2 shows that the iterative method obtains relatively accurate approximations*

to the true solutions. In practice, the interpolations performed in (3.16) are done on smooth functions, as visualized in Figure 5.3. The largest source of error from our proposed algorithm stems from the tensor decomposition, i.e., lines 1–17 in Algorithm 1. This can be seen, for example, in Figure 5.4. Conventional equidistant nodes construct the reduced order model from a variety of solutions.

4. Novel contribution of our approach. Clearly, the most expensive operations in Algorithm 1 are the inner products of two vectors of dimension n , and, thus, the cost of each step in the tensor decomposition scales linearly with the number of unknowns in (1.1). However, *the choice of nodes (3.2) has a very large influence on the overall expense of the decomposition.* In particular, the sampling determines how many iterations are taken until a fixed point is found and how many modes m are included in the reduced order model. If too many snapshots are included in the tensor matrix, the decomposition can fail to converge within expected time constraints.

The choice of nodes can also determine the quality of the resulting model. Specifically, the decomposition considered in this work is sensitive to *overfitting*. When overfitting occurs, the snapshots are well approximated by the model, but approximations corresponding to pairs of $(\mu_1, \mu_2) \notin \boldsymbol{\mu}$ are not acceptably accurate. Moreover, not including enough snapshots in the tensor matrix can be problematic. This scenario can result in high levels of error, as the model has not received enough information to capture the underlying structure of the solutions.

It is therefore advantageous to have access to solutions corresponding to many different pairs of (μ_1, μ_2) , as the initial selection rarely leads to a robust and accurate model. Further, it is not known a priori which sets of snapshots will produce acceptable models. *Our proposed method, which computes the snapshots as one-variable functions using Preconditioned Chebyshev BiCG, offers an effective means of generating a wide range of snapshots and, consequently, accurate models for parameterized linear systems.*

5. Numerical simulations of a parameterized Helmholtz equation. We consider both a reduced order model for a parameterized Helmholtz equation and a parameter estimation problem for the solution to a parameterized Helmholtz equation. Such settings occur naturally, for example, in the study of geophysics; see [28, 32, 34]. These prior works were also based on a reduced order model, constructed using PGD. Similarly, the method PGD was used in the study of thermal process in [1], and a reduced basis method for solving parameterized PDEs was considered in [20].

In the simulations which follow, the matrices A_i arise from a finite element discretization, and b is the corresponding load vector. All matrices and vectors here were generated using the finite element software FEniCS [3]. The solutions to these discretized systems were approximated with a modified version of the Krylov subspace method Preconditioned Chebyshev BiCG [14], as described in Section 2. This strategy requires a linear solve with a matrix of dimension $n \times n$ on each application of the preconditioner and of its adjoint. We have chosen to perform the linear solve by computing one LU decomposition per execution of the main algorithm, which is reused at each subsequent iteration accordingly. This can be avoided by considering the inexact version of Preconditioned Chebyshev BiCG, described in the original work.

This work proposes a novel improvement in generating snapshot solutions necessary for constructing models of this type. We choose to include three different examples in this section in order to fully capture the versatility of our strategy. Once the interpolation (3.16) has been constructed, evaluating the approximations for many values of the parameters μ_1 and μ_2 can be done in an efficient manner; see Remark 3.4.

In the case of the tensor decomposition failing to converge sufficiently or the model lacking accuracy outside of the original snapshots, a new set of approximations can be generated with little extra work. From these solutions, a new decomposition can be attempted; see Section 4.

5.1. First simulation, snapshots sampled on a sparse grid. Consider the Helmholtz equation given by

$$(5.1a) \quad \nabla^2 u(x) + f(\mu_1, \mu_2)u(x) = h(x), \quad x \in \Omega,$$

$$(5.1b) \quad u(x) = 0, \quad x \in \partial\Omega,$$

where $\Omega \subset \mathbb{R}^2$ is as in Figure 5.5, $\mu_1 \in [1, 2]$, $\mu_2 \in [1, 2]$, $f(\mu_1, \mu_2) = 2\pi^2 + \cos(\mu_1) + \mu_1^4 + \sin(\mu_2) + \mu_2$, and $h(x) = \sin(\pi x_1) \sin(\pi x_2)$. A discretization of (5.1) is of the form (1.1), where

$$A(\mu_1, \mu_2) := A_0 + f(\mu_1, \mu_2)A_1.$$

We are interested in approximating $u(x)$ in (5.1) for many different pairs of (μ_1, μ_2) simultaneously.

The reduced order model $\mathbf{X}^m(\mu_1, \mu_2)$ is constructed as described in Algorithm 1. We can evaluate this model for (μ_1, μ_2) outside of the nodes corresponding to the snapshot solutions. The particular 13 nodes considered in this simulation are plotted in the parameter space, shown in Figure 5.1. Figure 5.2 displays the convergence of the two executions of Preconditioned Chebyshev BiCG required to generate the snapshot corresponding to the nodes in Figure 5.1. Specifically, in Figure 5.2(a), we see faster convergence for approximations $\hat{x}(\mu_1, \mu_2^*)$ where the value μ_1 is closer to the target parameter σ in (2.4); see Remark 2.1. An analogous result holds in Figure 5.2(b). We require the LU decompositions of 2 different matrices of dimension $n \times n$ for this simulation.

In Figure 5.3, we see the interpolations $\mathbf{F}_1^1(\mu_1)$ and $\mathbf{F}_2^1(\mu_2)$ as in (3.16) plotted along with the function evaluations $F_1^1(\mu_1^i)$ and $F_2^1(\mu_2^j)$ generated by Algorithm 1, where μ_1^i and μ_2^j are as in Figure 5.1. Figure 5.4 shows the percent relative error for approximations to (5.1) for a variety of pairs (μ_1, μ_2) different from the nodes plotted in Figure 5.1. As in [26], we consider approximate solutions with percent relative error below 6% reliable and approximations with percent relative error below 1.5% accurate, where the error is computed by comparing the approximation to the solution obtained using backslash in MATLAB. Figures 5.5, 5.6, and 5.7 show both the exact finite element solution and the solution generated from (3.16) for the sake of comparison. Here we display these solutions for 3 pairs of (μ_1, μ_2) . These approximations all have percent relative error below 1.5%. A variety of solutions can be obtained from this reduced order model.

5.2. Second simulation, snapshots sampled on a full grid. To obtain an accurate model over the entire parameter space, we consider using HOPGD with sampling performed on a full grid. This is the approach taken in [8, 26] to approximate parametric PDEs. The snapshots are obtained using the Krylov subspace method described in Section 2, and the model is constructed in a way that is completely analogous to the method described in Section 3. As the decomposition is performed on a tensor matrix containing more snapshots, the method is more costly.

Specifically, we build a reduced order model to approximate the solution to the

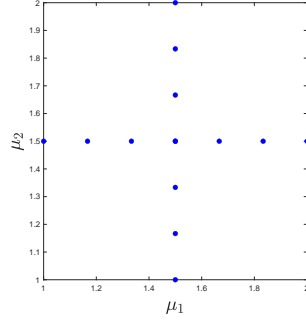


FIG. 5.1. Locations of 13 snapshots (μ_1^i, μ_2^*) and (μ_1^*, μ_2^j) used to construct X^m in (3.3) to approximate (5.1), sampling on a sparse grid in the parameter space.

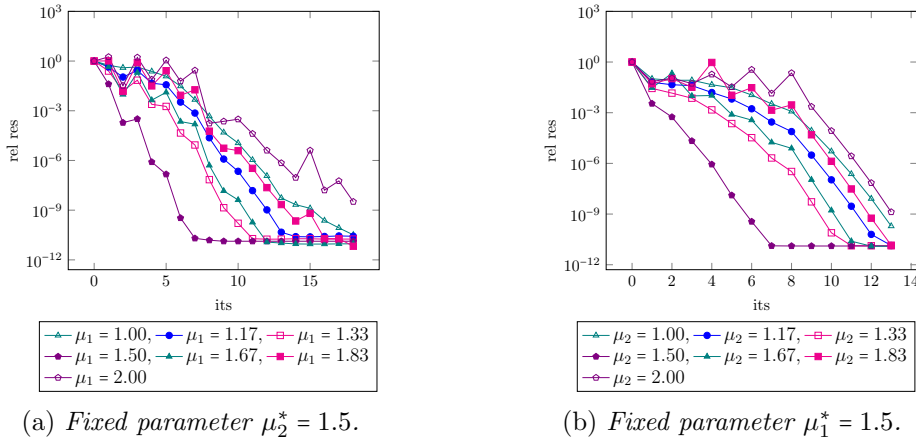


FIG. 5.2. Convergence of Preconditioned Chebyshev BiCG for generating the snapshot solutions corresponding to the nodes in Figure 5.1. Simulation in Figure 5.2(a) gives all solutions for (μ_1, μ_2^*) , $\mu_1 \in [1, 2]$, simulation in Figure 5.2(b) gives all solutions for (μ_1^*, μ_2) , $\mu_2 \in [1, 2]$.

Helmholtz equation given by

$$(5.2a) \quad (\nabla^2 + f_1(\mu_1) + f_2(\mu_2)\alpha(x))u(x) = h(x), \quad x \in \Omega,$$

$$(5.2b) \quad u(x) = 0, \quad x \in \partial\Omega,$$

where $\Omega \subset \mathbb{R}^2$ is as in Figure 5.9, $\alpha(x) = x_2$, $\mu_1 \in [1, 2]$, $\mu_2 \in [1, 2]$, and $f_1(\mu_1) = \cos(\mu_1) + \mu_1^3$, $f_2(\mu_2) = \sin(\mu_2) + \mu_2^2$, $h(x) = \sin(\pi x_1) \sin(\pi x_2)$. A discretization of (5.2) is of the form (1.1), where

$$A(\mu_1, \mu_2) := A_0 + f_1(\mu_1)A_1 + f_2(\mu_2)A_2,$$

and approximating $u(x)$ in (5.3) for many different pairs of (μ_1, μ_2) is of interest. We can still exploit the structure of the sampling when generating the snapshots by fixing one parameter and returning solutions as a one variable function of the

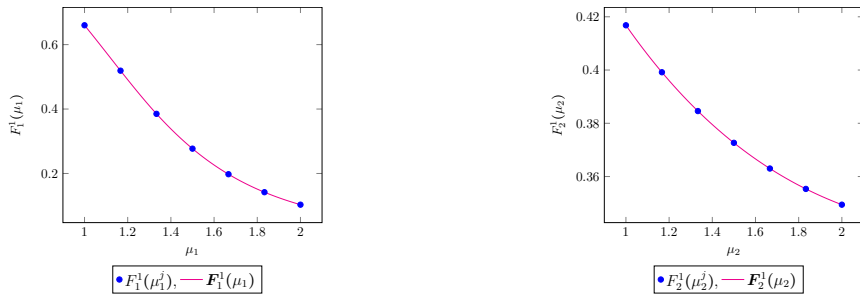


FIG. 5.3. Function evaluations $F_1^1(\mu_1^i)$ and $F_2^1(\mu_2^j)$ produced by Algorithm 1 to approximate (5.1), plotted with corresponding interpolations $\mathbf{F}_1^1(\mu_1)$ and $\mathbf{F}_2^1(\mu_2)$ as in (3.16) with μ_1^i and μ_2^j as in Figure 5.1.

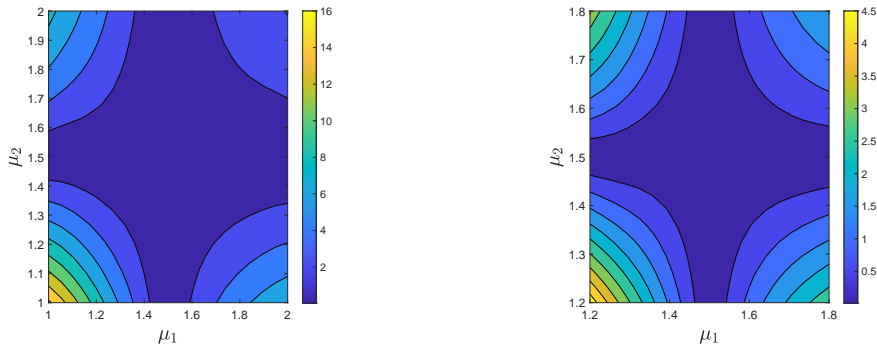
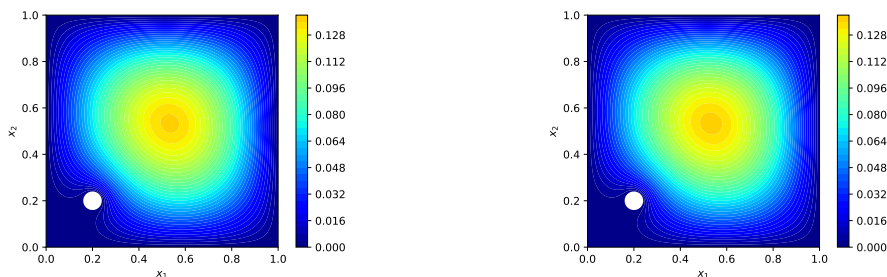


FIG. 5.4. Percent relative error of $x^m(\mu_1, \mu_2)$ (3.17) to approximate (5.1) for 400 equidistant pairs of (μ_1, μ_2) , $m = 14$, $n = 112995$. Here accurate: $< 1.5\%$, reliable: $< 6\%$. Note, same model in both figures.

other parameter. As in the simulations based on sampling on a sparse grid, if the decomposition fails to reach a certain accuracy level, or the model is inadequate due to overfitting or not enough data, a new set of snapshots can be generated with little extra computational effort. These solutions can be used to build a better model.

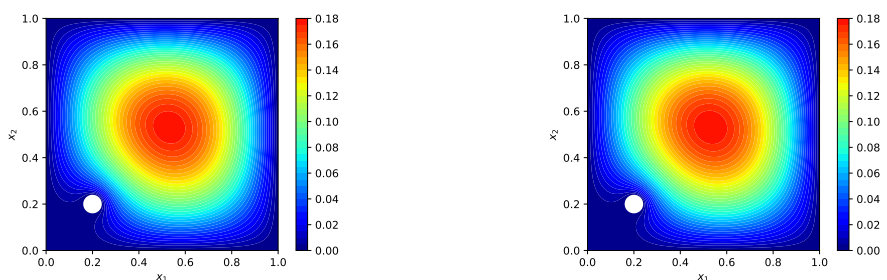
Figure 5.8(a) shows the locations of the nodes corresponding to 77 different snapshot solutions used to construct a reduced order model. These snapshots were generated via 7 executions of a modified form of Preconditioned Chebyshev BiCG, i.e., we consider 7 different fixed μ_2^* , equally spaced on $[a_2, b_2]$. This requires the LU decompositions of 7 different matrices of size $n \times n$. Figure 5.8(b) shows the percent relative error of the interpolated approximation, analogous to (3.16) constructed using Algorithm 1, for 400 pairs of $(\mu_1, \mu_2) \in [1, 2] \times [1, 2]$, different from the nodes corresponding to the snapshot solutions. We note that the percent relative error of the approximation is below 1% for all pairs (μ_1, μ_2) , indicating that the approximations are accurate. For the sake of comparison, Figures 5.9, 5.10 and 5.11 show both the exact finite element solutions and corresponding reduced order model solutions for 3 pairs of (μ_1, μ_2) . In general, accurate solutions can be produced on a larger parameter



(a) *Exact finite element solution*

(b) *Reduced order model solution*

FIG. 5.5. Approximation to (5.1) with $m = 14$, $n = 112995$, 0.347% relative error (accurate), $\mu_1 = 1.6$, $\mu_2 = 1.4$.



(a) *Exact finite element solution*

(b) *Reduced order model solution*

FIG. 5.6. Approximation to (5.1) with $m = 14$, $n = 112995$, 0.171% relative error (accurate), $\mu_1 = 1.45$, $\mu_2 = 1.6$.

space with sampling on a full grid.³ Furthermore, the model can produce a variety of solutions.

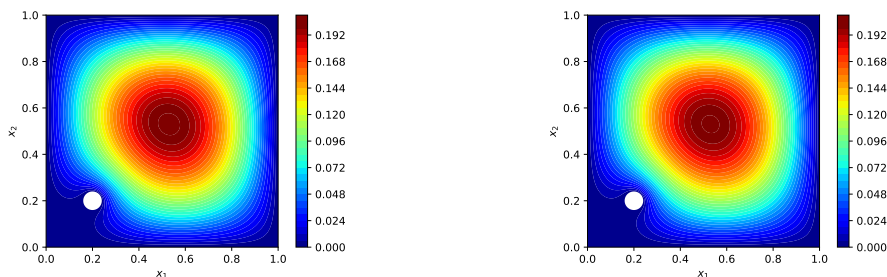
5.3. Third simulation, parameter estimation with snapshots sampled on a sparse grid. We consider now an application of our method to solve a parameter estimation problem. Similar methods have been constructed in the context of parameterized PDEs, for example, [27, 29, 32]. Our approach is analogous to the experiments performed in [27], where several reduced order models were constructed using the method sparse grid based HOPGD [25]. Consider the Helmholtz equation given by

$$(5.3a) \quad (\nabla^2 + f_1(\mu_1) + f_2(\mu_2)\alpha(x))u(x) = h(x), \quad x \in \Omega,$$

$$(5.3b) \quad u(x) = 0, \quad x \in \partial\Omega,$$

where $\Omega = [0, 1] \times [0, 1]$, $\alpha(x) = x_1$, $f_1(\mu_1) = \sin^2(\mu_1)$, $f_2(\mu_2) = \cos^2(\mu_2)$, $\mu_1 \in [0, 1]$, $\mu_2 \in [0, 1]$, and $h(x) = \exp(-x_1x_2)$. A discretization of (5.3) is of the form (1.1),

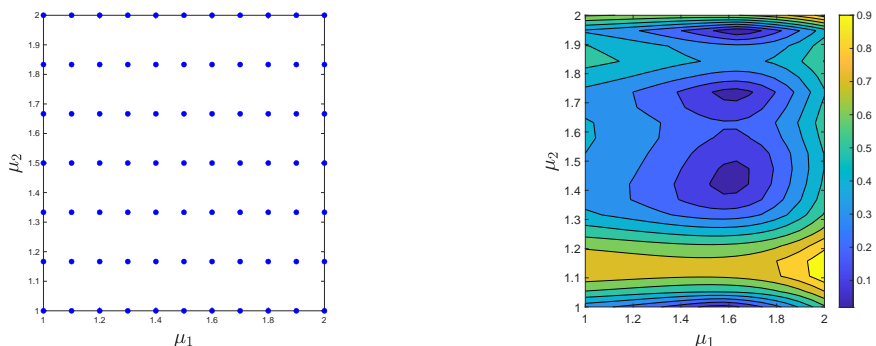
³See the adaptive refinement strategy proposed in [25], used to achieve accuracy on the full parameter space.



(a) *Exact finite element solution*

(b) *Reduced order model solution*

FIG. 5.7. Approximation to (5.1) with $m = 14$, $n = 112995$, 0.414% relative error (accurate), $\mu_1 = 1.4$, $\mu_2 = 1.4$.



(a) *77 nodes, corresponding snapshots generated via 7 executions of Preconditioned Chebyshev BiCG, 7 fixed values μ_2^* .*

(b) *Percent relative error of interpolation of reduced order model for 400 equidistant pairs of (μ_1, μ_2) .*

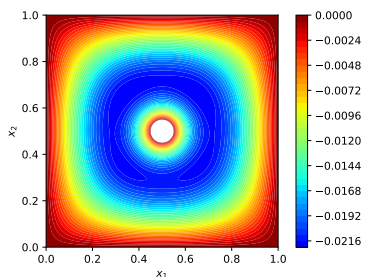
FIG. 5.8. Simulation for approximating (5.2). Here percent relative error $< 1.5\%$ (accurate), $n = 112693$, $m = 16$, sampling on a full grid.

where

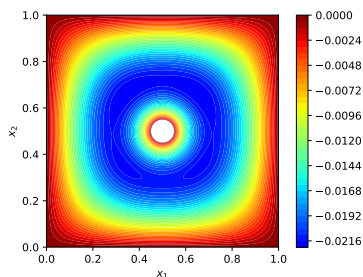
$$A(\mu_1, \mu_2) := A_0 + f_1(\mu_1)A_1 + f_2(\mu_2)A_2.$$

We consider a parameter estimation problem, i.e., we have a solution to the discretized problem, where the parameters (μ_1, μ_2) are unknown. In particular, the solution is obtained using backslash in MATLAB.

Figures 5.12(a), 5.12(b), and 5.12(c) together show a method similar to the one proposed in [27] for approximating this problem, performed by constructing 3 successive HOPGD models with sampling on sparse grids. This simulation executes a modified form of Preconditioned Chebyshev BiCG 6 times, requiring the LU factorizations of 6 different matrices of dimension $n \times n$ to generate the 39 snapshot solutions used to create the 3 reduced order models. Once the models have been constructed,

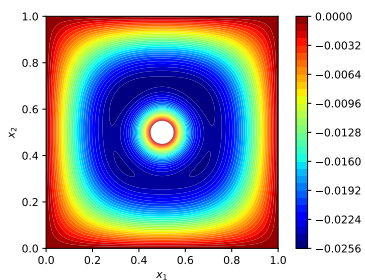


(a) *Exact finite element solution*

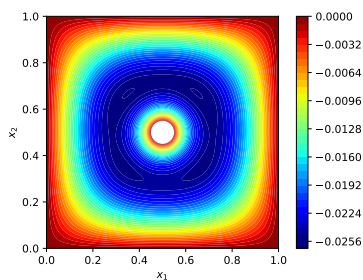


(b) *Reduced order model solution*

FIG. 5.9. *Approximation to (5.2) with $m = 16$, $n = 112693$, 0.340% relative error (accurate), $\mu_1 = 1$, $\mu_2 = 1$.*



(a) *Exact finite element solution*



(b) *Reduced order model solution*

FIG. 5.10. *Approximation to (5.2) with $m = 16$, $n = 112693$, 0.714% relative error (accurate), $\mu_1 = 1.8$, $\mu_2 = 1.2$.*

an interpolation is performed, followed by the minimization of (3.18). Table 5.1 shows the percent relative error in the estimated values of μ_1 and μ_2 for each run. Each execution of our strategy leads to a better estimation of the pair of parameters. As before, if the decomposition fails to reach a certain level of accuracy on a set of snapshots, or the model is lacking in robustness, a new set of approximations in the same parameter space can be generated with little extra computational effort. These solutions can be used in order to construct a better model.

	rel err % μ_1	rel err % μ_2
First run, $m = 34$	41.87417	97.40212
Second run, $m = 25$	2.66555	105.09263
Third run, $m = 7$	0.05706	1.69921

Table 5.1: *Percent relative error for parameter estimation in μ_1 and μ_2 for solution to (5.3), $n = 10024$.*

6. Numerical simulations of a parameterized advection-diffusion equation. The advection-diffusion equation can be used to model particle transport, for

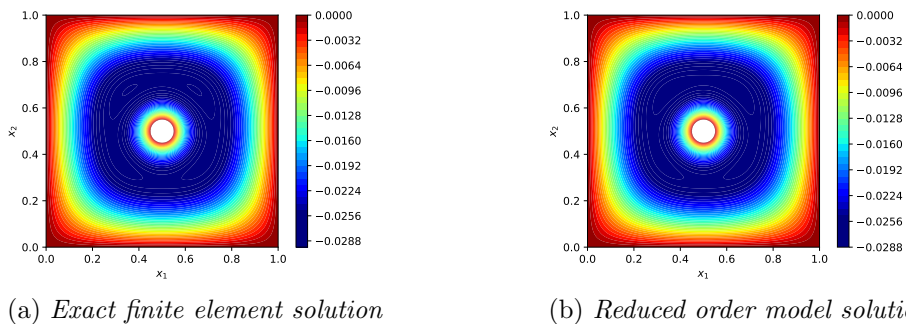


FIG. 5.11. Approximation to (5.2) with $m = 16$, $n = 112693$, 0.946% relative error (accurate), $\mu_1 = 2$, $\mu_2 = 2$.

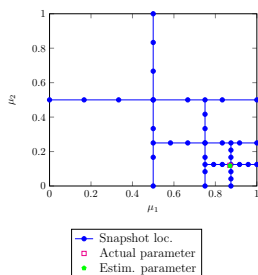
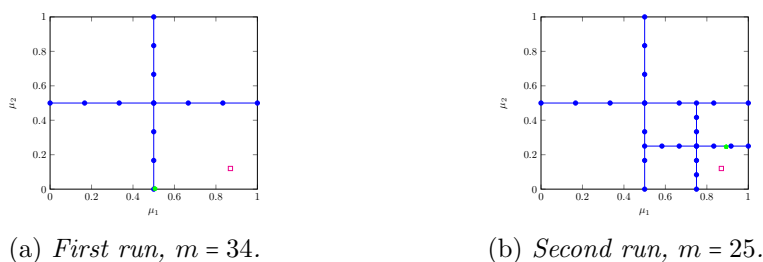


FIG. 5.12. Parameter estimation for solution to (5.3), $n = 10024$.

example the distribution of air pollutants in the atmosphere; see [17, 33]. In particular, we consider the parameterized advection-diffusion equation given by

$$(6.1) \quad \frac{\partial}{\partial t} u(x, t) = f_1(\mu_1) \frac{\partial^2}{\partial x^2} u(x, t) + f_2(\mu_2) \frac{\partial}{\partial x} u(x, t),$$

where $f_1(\mu_1) = 1 + \sin(\mu_1)$, $f_2(\mu_2) = 10 + \cos(\mu_2) + \pi\mu_2$ and $x \in [0, 1]$, $t \in [0, T]$. The boundary conditions $u(0, t) = 0$, $u(1, t) = 0$ are enforced, as well as the initial condition $u_0(x) = u(x, 0) = \sin(\pi x)$. Here, $f_1(\mu_1)$ is referred to as the diffusion coefficient, and the value $f_2(\mu_2)$ is the advection parameter. Discretizing (6.1) in space, with a finite difference scheme, and in time, with the implicit Euler method, gives a parameterized

linear system of the form (1.1), where

$$A(\mu_1, \mu_2) := A_0 + f_1(\mu_1)A_1 + f_2(\mu_2)A_2.$$

Note, the solution to this linear system gives an approximation to (6.1) at a specific discrete time-step. As in Section 5, we construct a reduced order model via a tensor decomposition [25], where the snapshots are generated efficiently with a modified version of the method Preconditioned Chebyshev BiCG [14]. Here the sampling is performed on a sparse grid in the parameter space. If the tensor decomposition is not successful or the resulting model is not sufficiently accurate, a new set of snapshots can be generated on the same parameter space with little extra computation. These solutions can be used to attempt to build a better model. Similar model problems appear in, for example, [31], where the method PGD was used to construct approximate solutions to the parameterized PDE. Once the corresponding reduced order model (3.16) has been constructed, approximating the solutions for many (μ_1, μ_2) can be done very cheaply; see Remark 3.4.

6.1. First simulation, snapshots sampled on a sparse grid. We construct approximations to (6.1) with Algorithm 1, where the sampling is performed as displayed in Figure 6.2(a). Figure 6.1 shows the percent relative error for approximations to (6.1) for 400 different pairs $(\mu_1, \mu_2) \in [0, 0.5] \times [0, 0.5]$, where, specifically, we consider the solutions at $t = 0.01$. As in [26], approximate solutions with percent relative error below 6% are considered reliable, and approximations with percent relative error below 1.5% are considered accurate. Here the error is computed by comparing the approximation to the solution obtained using backslash in MATLAB. The 9 snapshots used to construct the reduced order model here were generated with 2 executions of Chebyshev BiCG, requiring the LU decompositions of 2 matrices of dimension $n \times n$.

Note, solutions to the advection-diffusion equation (6.1) are time-dependent. An all-at-once procedure could be utilized to approximate solutions to this equation at many different time-steps, though this approach would result in a larger number of unknowns and a longer simulation time. Alternatively, the decomposition could be modified to construct an approximation similar to the one in (3.3), separated in the time variable t as well as the parameters μ_1 and μ_2 . Such an approach would, however, require specific testing. Furthermore, a decomposition of this form performed with HOPGD sampling on a sparse grid in the parameter space may not be optimal [25].

6.2. Second simulation, parameter estimation with snapshots sampled on a sparse grid. Consider again a parameter estimation problem. Specifically, we have an approximation to $u(x, t) \in \mathbb{R}^n$ in (6.1), where $t = 0.01$ is known, but the parameters μ_1 and μ_2 are not. This approximation corresponds to the solution to the discretized problem and is obtained using backslash in MATLAB. Additionally, there is some uncertainty in the measurement of the given solution. In this way, we express our observed solution $u^{\text{obs}} \in \mathbb{R}^n$ as

$$(6.2) \quad u^{\text{obs}} := u(x, t) + \varepsilon \Delta,$$

where $\Delta \in \mathcal{N}(0, I) \in \mathbb{R}^n$ is a random vector and $\varepsilon = 10^{-2}$.

Figure 6.2 and Table 6.1 show the result of this parameter estimation problem, using a similar strategy to the one described in [27]. Here 3 successive HOPGD models are constructed from snapshots sampled on a sparse grid in the parameter space $(\mu_1, \mu_2) \in [0, 0.5] \times [0, 0.5]$. This simulation executes a modified version of Chebyshev BiCG 6 times, generating the 23 snapshots efficiently. Note, this requires

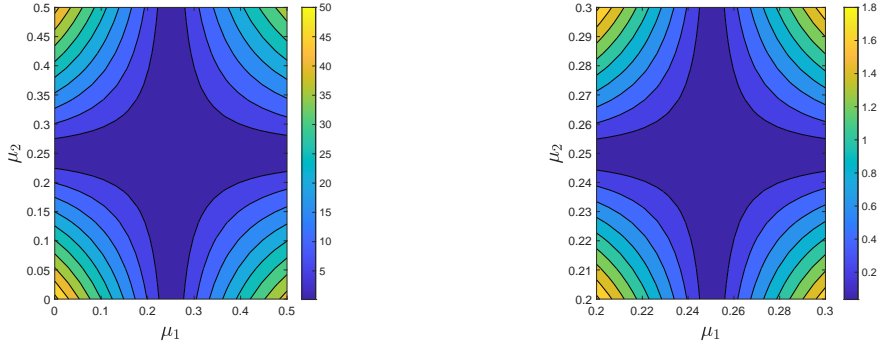
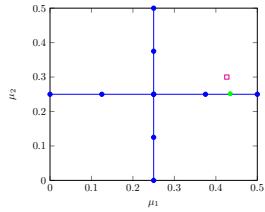
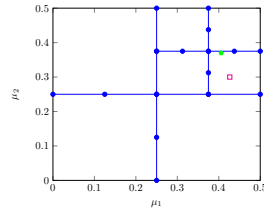


FIG. 6.1. Percent relative error of $x^m(\mu_1, \mu_2)$ (3.17) to approximate (6.1) for 400 pairs of (μ_1, μ_2) , $m = 50$, $n = 9999$. Here accurate: $< 1.5\%$, reliable $< 6\%$. Note, same model in both figures.

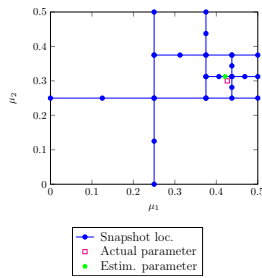
the LU decompositions of 6 matrices of dimension $n \times n$. After the third run of Algorithm 1, the estimated parameter is very close to the actual parameter. Note, the relative error in μ_1 and μ_2 after the third run of the simulation is of the same order of magnitude as the noise in the observed solution (6.2).



(a) First run, $m = 50$.



(b) Second run, $m = 25$.



(c) Third run, $m = 15$.

FIG. 6.2. Parameter estimation for noisy solution to (6.1), $n = 9999$.

	rel err % μ_1	rel err % μ_2
First run, $m = 50$	1.9004	16.1248
Second run, $m = 25$	4.8542	23.2504
Third run, $m = 15$	1.2313	4.2588

Table 6.1: Percent relative error for parameter estimation in μ_1 and μ_2 for noisy solution to (6.1), $n = 9999$.

7. Conclusions and future work. This work proposes a novel way to generate the snapshot solutions required to build a reduced order model. The model is based on an efficient decomposition of a tensor matrix, where the sampling is performed on a sparse grid. An adaptation of the previously proposed method Preconditioned Chebyshev BiCG is used to generate many snapshots simultaneously.

Tensor decompositions may fail to reach a certain level of accuracy on a given set of snapshot solutions. Further, reduced order models based on sampling can suffer from overfitting, and the choice of snapshots can affect the simulation time. Our approach offers a way to generate a new set of snapshots on the same parameter space with little extra computation. This is advantageous, as it is not known a priori if a given set of snapshots will produce an accurate and robust model, and generating snapshots is computationally demanding in general. The reduced order model can also be used to solve a parameter estimation problem. Numerical simulations show competitive results.

In [25], a residual-based accelerator was used in order to decrease the number of iterations required by the fixed point method when computing the updates described in (3.10), (3.12), and (3.13). Techniques of this variety are especially effective when the snapshot solutions have a strong dependence on the parameters. Such a strategy could be directly incorporated into this work, though specific testing of the effectiveness would be required.

8. Acknowledgements. The Erasmus+ programme of the European Union funded the first author’s extended visit to Trinity College Dublin to carry out this research. The authors thank Elias Jarlebring (KTH Royal Institute of Technology) for fruitful discussions and for providing feedback on the manuscript. Additionally, the authors wish to thank Anna-Karin Tornberg (KTH Royal Institute of Technology) and her research group for many supportive, constructive discussions.

REFERENCES

- [1] J. V. AGUADO, A. HUERTA, F. CHINESTA, AND E. CUETO, *Real-time monitoring of thermal processes by reduced-order modeling*, Internat. J. Numer. Methods Engrg., 102 (2015), pp. 991–1017.
- [2] M. I. AHMAD, D. B. SZYLD, AND M. B. VAN GIJZEN, *Preconditioned multishift BiCG for \mathcal{H}_2 -optimal model reduction*, SIAM J. Matrix Anal. Appl., 38 (2017), pp. 401–424.
- [3] M. S. ALNAES, J. BLECHTA, J. HAKE, A. JOHANSSON, B. KEHLET, A. LOGG, C. RICHARDSON, J. RING, M. E. ROGNES, AND G. N. WELLS, *The FEniCS project version 1.5*, Arch. Numer. Softw., 3 (2015).
- [4] A. AMIRASLANI, R. M. CORLESS, AND P. LANCASTER, *Linearization of matrix polynomials expressed in polynomial bases*, IMA J. Numer. Anal., 29 (2009), pp. 141–157.
- [5] A. AMMAR, B. MOKDAD, F. CHINESTA, AND R. KEUNINGS, *A new family of solvers for some classes of multidimensional partial differential equations encountered in kinetic theory modelling of complex fluids*, J. Non-Newtonian Fluid Mech., 139 (2006), pp. 153–176.
- [6] ———, *A new family of solvers for some classes of multidimensional partial differential equa-*

- tions encountered in kinetic theory modelling of complex fluids. Part II: Transient simulation using space-time separated representations, *J. Non-Newtonian Fluid Mech.*, 144 (2007), pp. 98–121.
- [7] G. BERKOOZ, P. HOLMES, AND J. L. LUMLEY, *The proper orthogonal decomposition in the analysis of turbulent flows*, *Annu. Rev. Fluid Mech.*, 25 (1993), pp. 539–575.
- [8] N. BLAL AND A. GRAVOUIL, *Non-intrusive data learning based computational homogenization of materials with uncertainties*, *Comput. Mech.*, 64 (2019), pp. 807–828.
- [9] D. BORZACCHIELLO, J. AGUADO, AND F. CHINESTA, *Non-intrusive sparse subspace learning for parameterized problems*, *Arch. Comput. Methods Eng.*, 26 (2017), pp. 303–326.
- [10] H. J. BUNGARTZ AND M. GRIEBEL, *Sparse grids*, *Acta Numer.*, 31 (2004), pp. 147–269.
- [11] F. CHINESTA, A. AMMAR, AND E. CUETO, *Recent advances and new challenges in the use of the proper generalized decomposition for solving multidimensional models*, *Arch. Comput. Methods Eng.*, 17 (2010), pp. 327–350.
- [12] F. CHINESTA, A. AMMAR, A. LEYGUE, AND R. KEUNINGS, *An overview of the proper generalized decomposition with applications in computational rheology*, *J. Non-Newtonian Fluid Mech.*, 116 (2011), pp. 578–592.
- [13] F. CHINESTA, P. LADEVEZE, AND E. CUETO, *A short review on model order reduction based on proper generalized decomposition*, *Arch. Comput. Methods Eng.*, 18 (2011), pp. 395–404.
- [14] S. CORRENTY, E. JARLEBRING, AND D. B. SZYLD, *Preconditioned Chebyshev BiCG method for parameterized linear systems*, *Electron. Trans. Numer. Anal.*, 58 (2023), pp. 629–656.
- [15] T. A. DRISCOLL, N. HALE, AND L. N. TREFETHEN, eds., *Chebfun Guide*, Pafnuty Publications, Oxford, 2014.
- [16] C. EFFENBERGER AND D. KRESSNER, *Chebyshev interpolation for nonlinear eigenvalue problems*, *BIT*, 52 (2012), pp. 933–951.
- [17] B. A. EGAN AND J. R. MAHONEY, *Numerical modeling of advection and diffusion of urban area source pollutants*, *J. Appl. Meteorol.* (1962-1982), 11 (1972), pp. 312–322.
- [18] R. FLETCHER, *Conjugate gradient methods for indefinite systems*, in *Numerical Analysis*, G. A. Watson, ed., Lecture Notes in Math., Vol. 506, Springer, Berlin, 1976, pp. 73–89.
- [19] A. FROMMER, *BiCGStab(ℓ) for families of shifted linear systems*, *Computing*, 70 (2003), pp. 87–109.
- [20] B. HAASDONK, M. OHLBERGER, AND G. ROZZA, *A reduced basis method for evolution schemes with parameter-dependent explicit operators*, *Electron. Trans. Numer. Anal.*, 32 (2008), pp. 145–161.
- [21] T. G. KOLDA AND B. W. BADER, *Tensor decompositions and applications*, *SIAM Rev.*, 51 (2009), pp. 455–500.
- [22] D. KRESSNER AND J. E. ROMAN, *Memory-efficient Arnoldi algorithms for linearizations of matrix polynomials in Chebyshev basis*, *Numer. Linear Algebra Appl.*, 21 (2014), pp. 569–588.
- [23] C. LANCZOS, *Solution of linear equations by minimized iterations*, *J. Res. Natl. Bur. Stand.*, 49 (1952), pp. 33–53.
- [24] L. D. LATHAUWER, B. D. MOOR, AND J. VANDEWALLE, *A multilinear singular value decomposition*, *SIAM J. Matrix Anal. Appl.*, 21 (2000), pp. 1253–1278.
- [25] Y. LU, N. BLAL, AND A. GRAVOUIL, *Adaptive sparse grid based HOPGD: Toward a nonintrusive strategy for constructing a space-time welding computational vademecum*, *Internat. J. Numer. Methods Engrg.*, 114 (2018), pp. 1438–1461.
- [26] ———, *Multi-parametric space-time computational vademecum for parametric studies: Application to real time welding simulations*, *Finite Elem. Anal. Des.*, 139 (2018), pp. 62–72.
- [27] ———, *Datadriven HOPGD based computational vademecum for welding parameter identification*, *Comput. Mech.*, 64 (2019), pp. 47–62.
- [28] D. MODESTO, S. ZLOTNIK, AND A. HUERTA, *Proper generalized decomposition for parameterized Helmholtz problems in heterogeneous and unbounded domains: Application to harbor agitation*, *Comput. Methods Appl. Mech. Engrg.*, 295 (2015), pp. 127–149.
- [29] E. NADAL, F. CHINESTA, P. DÍEZ, F. J. FUENMAYOR, AND F. D. DENIA, *Real time parameter identification and solution reconstruction from experimental data using the proper generalized decomposition*, *Comput. Methods Appl. Mech. Engrg.*, 296 (2015), pp. 113–128.
- [30] J. NOCEDAL AND S. WRIGHT, *Numerical Optimization*, Springer Series, 2006.
- [31] A. NOUY, *A priori model reduction through Proper Generalized Decomposition for solving time-dependent partial differential equations*, *Comput. Methods Appl. Mech. Engrg.*, 199 (2010), pp. 1603–1626.
- [32] M. SIGNORINI, S. ZLOTNIK, AND P. DÍEZ, *Proper Generalized Decomposition solution of the parameterized Helmholtz problem: application to inverse geophysical problems*, *Internat. J. Numer. Methods Engrg.*, 109:8 (2017), pp. 1085–1102.

- [33] S. ULFAH, S. A. AWALLUDIN, AND WAHIDIN, *Advection-diffusion model for the simulation of air pollution distribution from a point source emission*, J. Phys.: Conf. Ser., 948 (2018), p. 012067.
- [34] S. ZLOTNIK, P. DÍEZ, D. MODESTO, AND A. HUERTA, *Proper generalized decomposition of a geometrically parameterized heat problem with geophysical applications*, Internat. J. Numer. Methods Engrg., 103 (2015), pp. 737–758.